# Operator Coexistence in IRS-Assisted mmWave Networks: A Wideband Approach

Joana Angjo\*, Anatolij Zubow, Falko Dressler

School of Electrical Engineering and Computer Science, TU Berlin, Germany

### Abstract

In sixth generation (6G) mobile networks, the push toward high-frequency bands for ultra-fast data rates intensifies the challenges of signal attenuation and reduced coverage range. Intelligent reconfigurable surfaces (IRSs) present a promising solution to these challenges by enhancing signal coverage and directing reflections, which also contribute to minimize loss. However, there are multiple challenges associated with IRS, which have to be addressed before full incorporation of this technology into existing networks. A key issue arises from the inability of IRS to filter out non-target signals from other frequency bands due to lack of bandpass filtering. In areas where multiple wireless operators are spatially nearby, even if they use different frequency bands, this may cause unwanted reflections that may degrade their communication performances. To address this challenge, we previously proposed a solution, which relied on partitioning an IRS into sub-surfaces (sub\_IRS) and dynamically assigning operators to these sub\_IRS. Results have shown that a proper assignment of wireless operators to sub\_IRS can improve the overall performance compared to a random assignment. In this paper, we introduce a wideband approach, demonstrating that the impact from unwanted reflections can be mitigated by using wideband channels, as the average signal to noise ratio (SNR) across subcarriers is less adversely affected. This approach leverages frequency diversity to reduce SNR variance, as some of the subcarriers may be negatively affected while others benefit, resulting in maintaining a more consistent and robust system performance in the presence of IRS-induced unwanted reflections. Simulations and real-world measurements confirm that the deployment of wideband IRS provides a robust strategy for combating inter-operator reflections in next generation IRS-assisted networks. Additionally, the wideband approach comes at no additional necessity for centralized resource control in future multi-operator networks. According to simulations, the SNR variance for a 1.28 GHz channel is approximately 20 dB lower than that of a 10 MHz channel when coexistence is considered. Similarly, measurements confirm a threefold reduction in SNR variation when transitioning from narrowband (10 MHz) to wideband (320 MHz) transmission. In overall, the usage of wideband channels in this context allows the system to be more stable and predictable.

Keywords: 6G, coexistence, IRS, RIS, intelligent reconfigurable surfaces, wireless operator coexistence, wideband

#### 1. Introduction

With the ever-growing demands for faster, more reliable connectivity, the move to higher frequencies is fundamental for future communication networks. Due to spectrum availability, these frequencies enable reaching ultra-high data rates that could power the target applications of sixth generation (6G) and beyond; from real-time holographic imaging to vast networks of autonomous vehicles [1]. However, these gains come at a cost, as high-frequency signals require line-of-sight (LOS) as they are more susceptible to obstacles and attenuation, significantly limiting communication range and resilience [2]. For these reasons, ongoing efforts are being made to address the challenges and harness the potential of these bands without compromising network resilience. One solution to overcome path loss

To address some of these limitations, intelligent reconfigurable surface (IRS) has emerged as a compelling alternative in 6G and beyond networks [8]. IRS is also referred to as reconfigurable intelligent surface (RIS) in the literature, and both terms are used interchangeably. In this text, however, we consistently adopt the former notation. Unlike massive MIMO, which relies on active antenna

and attenuation is to perform intensive beamforming, such that the signal is focused precisely toward the intended receiver, maximizing signal strength in the target direction while also reducing interference elsewhere [3]. Multiple-input multiple-output (MIMO) and massive MIMO are promising solutions, as they employ a large number of active antennas to enable spatial multiplexing and high data rates [4–6]. However, despite its advantages, massive MIMO requires significant power, complex processing, and substantial infrastructure, which can be challenging to implement, especially at higher frequency bands where hardware costs are higher and power efficiency is critical [7].

<sup>\*</sup>Corresponding author

Email addresses: angjo@ccs-labs.org (Joana Angjo), zubow@ccs-labs.org (Anatolij Zubow), dressler@ccs-labs.org (Falko Dressler)

arrays, an IRS employs passive, programmable elements to reflect or redirect incoming signals. This passive design enables IRS to operate with much lower power consumption, reducing both hardware complexity and operating costs while still improving network efficiency. As a result, IRS has become a focal point of research due to its potential to expand signal coverage and create adaptable communication environments [9, 10]. This potential is reflected not only theoretically, but also in practical implementations and manufacture: different IRS-assisted setups operating at different frequencies are reported in [11]. Various technologies have been developed to manufacture IRS prototypes, such as 3D printing for passive metasurfaces in the millimeter wave (mmWave) band [12], printed circuit board (PCB) technology with tunable elements for 5 GHz prototypes [13], and liquid crystal-based designs demonstrated at 62 GHz [14]. Recent advancements of IRS even show its ability to perform analog-domain operations like Fourier transforms, enabling integrated communication and processing.

However, the incorporation of IRS into future networks does not come without its challenges [15], which mainly include hardware limitations like discrete and phasedependent reflection control, mutual coupling between elements, and complex channel estimation. Additionally, practical deployment issues such as frequency band leakage, inter-operator interference, and difficulties with large-scale control must be addressed for widespread adoption [16]. For instance, one of the most elaborated obstacles of IRS implementation is the dynamic optimization of its elements. Since an IRS typically does not generate or amplify signals, it relies on the cascaded path created by the initial transmission and its subsequent reflection. It is noteworthy to mention that active IRS variants are also feasible [17], however, passive IRS is preferred for its energy efficiency advantage over massive MIMO. The dual-hop process complicates channel estimation, as accurate knowledge of both direct and reflected paths is essential for optimizing the phase shifts of each element. Consequently, developing efficient and reliable methods for channel estimation and IRS configuration remains critical to unlocking its full potential in future networks [18].

Other challenges emerge in densely deployed network scenarios, where multiple operators must manage interference and spectrum allocation efficiently. In fifth generation (5G) mobile networks, coexistence among operators is achieved through frequency planning, where each provider is assigned dedicated spectrum bands, eliminating the need for real-time coordination and effectively preventing interference [20]. However, with the introduction of IRS, this method may become insufficient and less effective. The potential for real-time reconfiguration of IRS introduces new dynamic and frequency-specific reflections, necessitating more advanced coordination strategies. Thus, a complex aspect of IRS technology is the coexistence of multiple IRSassisted networks operating at different frequency bands in close proximity [21, Section 6.7.2]. Because IRS is typically optimized for a specific frequency band and it does not

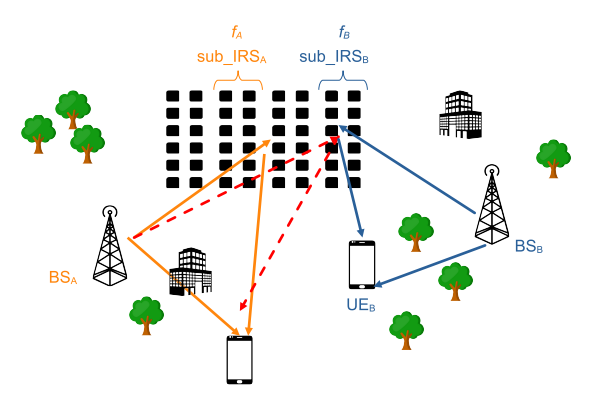


Figure 1: Two operators are assigned to a sub\_IRS each. The solid line arrows represent the wanted reflections, whereas the dashed line the unwanted reflection ([19, Section III]).

have bandpass filtering capabilities [22], there is a potential for unintended reflections and interactions when different bands are used nearby. Understanding how IRS configuration for one frequency impacts other signals is crucial, as optimization for one network may adversely affect others. Furthermore, in mobile scenarios, the reconfiguration of IRS leads to temporal changes in multipath characteristics, causing artificial signal fading. Unlike typical multipath reflections, IRS reflections are engineered for precise phase and amplitude control at a specific frequency. As a result, even small frequency variations can lead to unintended phase shifts and altered reflection characteristics.

A potential solution would be to place IRSs far apart from each other to minimize the likelihood of unwanted reflections. However, in practice, operators often densely deploy their base stations (BSs), particularly in urban areas, where network capacity demands require closer infrastructure placement. In some cases, multiple operators even share the same BS towers to reduce deployment costs and improve coverage efficiency [23]. In such scenarios, unwanted reflections can become particularly detrimental, further complicating unwanted reflections management. Without coordination, operators managing their IRSs independently may lead to inefficient use of IRSs as a shared resource, creating a situation analogous to the "Tragedy of the Commons" [24].

Our previous studies have analyzed the coexistence of different operators in IRS-assisted networks. In [19], we examined a network with multiple operators using a single centralized IRS. In contrast, [25] explored a distributed IRSs system. The core idea in both studies is similar: in the former, we proposed a solution in the spatial domain: dividing the IRS into sub-surfaces (sub\_IRSs), which are dynamically assigned to operators based on demand and potential impact on neighboring networks. A schematic representation of the system model used in the former work is shown in Fig. 1. Here, a centralized IRS is split into multiple sub\_IRSs, and the operators denoted by a BS and a single user equipment (UE) (where the subscript

denotes the network nodes of an operator) are assigned to one of these sub\_IRSs. Each sub\_IRS is configured to optimally direct the signal toward the receiver (Rx), with the desired reflections indicated by solid arrows. However, since each sub\_IRS reflects all incoming signals, the signal from operator A is also reflected by  $sub_IRS_B$  (and vice versa). Our results show that properly assigning operators to sub\_IRS units can mitigate the effect of unwanted reflections, resulting in improved overall system performance of sum rate (SR) and fairness in terms of data rates, compared to static or random assignment methods. Similar results in [25] confirmed that in a distributed IRSs setup, sub\_IRSs allocation outperformed the traditional one-IRS-per-operator assignment. These findings suggest that cooperative strategies can effectively mitigate coexistence challenges in IRS-assisted networks.

The aforementioned solutions may be difficult to implement, particularly in systems involving mobility. For this reason, we explore alternative approaches that do not rely on direct system modifications or complex control mechanisms. We hypothesize that in wideband channels, the average signal to noise ratio (SNR) across subcarriers is less negatively impacted by unwanted IRS reflections compared to narrowband channels. While certain subcarriers may still suffer from destructive interference, others can benefit from constructive effects, leading to an overall averaging that improves performance. Therefore we propose leveraging wideband operation as a natural and practical way to mitigate the negative effects of unwanted reflections for keeping the network's performance more stable and more predictable. This approach also aligns with the trend in future communication systems toward higher frequencies, where wider bandwidth (BW) is readily available and crucial for achieving ultra-high data rates.

As a valuable byproduct of this investigation, we also gain insights into IRS behavior under wideband operation. Most prior studies have focused on narrowband transmissions in the mmWave regime, for instance, we have used 10 MHz signals at 28 GHz in our previous study. Similarly, much of the existing IRS literature either considers narrowband systems or, in the case of orthogonal frequency division multiplexing (OFDM)-based studies, assumes frequency-independent reflections across wide bandwidths (e.g., [26]). However, this assumption does not hold in practice, as recent studies (e.g., [27]) have demonstrated that IRS reflections are in fact frequency-dependent in wideband scenarios.

To support our hypothesis, we perform simulations in MATLAB for a wideband IRS-assisted wireless network and demonstrate that the impact of unwanted reflections indeed diminishes with wider BWs. Additionally, using a real testbed at 28 GHz composed of software defined radio (SDR), specifically universal software radio peripheral (USRP) X410 devices and non-reconfigurable reflecting surface (NRRS), we show that these results also hold in practice. NRRSs operate similarly to IRSs by reflecting an incoming signal in a designated direction; however, they

are pre-configured and lack the capability to dynamically adjust their reflection direction. Thus, they provide a relatively cost-effective solution for creating artificial signal paths. The simulations examine the coexistence of operators for BWs up to 1.28 GHz, while the testbed operates at a 320 MHz BW, both in the 28 GHz frequency regime. As expected, higher BWs exhibit increased frequency selectivity. We demonstrate that employing advanced PHY layers, such as 802.11be, can effectively help mitigate this effect.

Our main contributions can be summarized as follows:

- We provide a comprehensive literature review on operator coexistence in IRS-assisted networks, which helps us formulate the hypothesis that the impact of unwanted reflections is reduced when the channel is wideband.
- We perform simulations to analyze the coexistence of multiple operators assisted by IRSs.
- We implement an experimental communication setup with the help of NRRSs to validate the simulation results.
- We present results confirming that the operator coexistence problem is less pronounced in wideband transmissions.

The rest of the paper is structured as follows. Section 2 provides an overview of the related work, with a focus on the coexistence of operators in IRS-assisted networks. Moreover, our previously proposed solution is revisited and the results are summarized. Next, the system model used in simulations and the real-time testbed of this paper are introduced in Section 3. The evaluation of the results is given in Section 4, and lastly the concluding remarks and discussions are found in Section 5.

# 2. Related Work

In this section, we first provide a summary of the coexistence problem among operators in IRS-assisted networks. Then, we revisit our previous works and summarize the main results, laying the groundwork for the system model of this paper.

# 2.1. Operator Coexistence Problem

In addressing inter-operator interference, a foundational study in [28] investigates the coexistence challenges introduced by IRS deployment. The authors propose two methods to manage "non-target signals", or as denoted before, the undesired reflections. The first solution leverages a multilayer meta-surface structure, where the initial layer acts as a bandpass filter, allowing only "target" signals to pass through to the second layer, where the IRS coefficients are applied. However, this approach has drawbacks, as the filter layer introduces additional costs and causes some power loss in the "target" signal. The second approach involves

Solution	Domain	Description	Limitation
Spectral filtering [28]	Frequency	An out-of-band frequency filtering layer on top of the IRS.	Increases cost and may deteriorate intended signal's quality.
Orthogonal IRS configurations during pilot transmission [29, 30]	Spatial	Assigning orthogonal IRS configurations during uplink pilot transmission to mitigate inter-operator pilot contamination.	Requires additional inter-operator information exchange and orchestration.
Ultra-narrowband metasurfaces	Frequency	Extreme frequency selectivity, allowing IRS elements to only interact with certain frequency bands.	High manufacturing complexity and cost.
Usage of typical IRS in combination with absorptive IRS [31]	Temporal	Dynamically switching the IRS to absorption mode when it is not used by the intended operator, in order to avoid interference.	Introduced complexity and costs due to the scheduling requirements.
Hierarchical deep reinforcement learning for IRS management and scheduling [32]	Temporal (primary)	Using hierarchical deep learning to optimize IRS allocation, beamforming, and user association over time, ensuring dynamic operator coordination.	High computational complexity and real-time adaptation challenges in large-scale IRS deployments.
sub_IRS assignment [19, 25, 28]	Spatial	Splitting the IRS into sub_IRSs and dynamically assigning them to operators.	Requires coordination between operators.
This work	Frequency	Wideband transmissions naturally mitigate coexistence effect.	The channel is more selective in wideband, necessitating usage of advanced physical layer protocols, like 802.11be.

Table 1: Classification of proposed solutions to mitigate unwanted interference in unintended frequency bands caused by IRS.

allocating different subblocks (sub\_IRSs) of an IRS to different operators, enabling each subblock to independently tune and beamform signals from specific operators. The authors suggest that using narrower beams can enhance performance by minimizing signal spillover into subblocks designated for other operators. However, beamwidth is frequency-dependent, and in real-world scenarios, antennas generate side-lobes, which can reduce the effectiveness of this method in achieving optimal performance. We then use this approach in [19, 25], showing that a proper assignment of operators to the sub\_IRSs can minimize the negative impacts of the unwanted inter-operator reflections. These works are elaborated in detail in Section 2.2.

The authors in [29, 30] discuss the inter-operator pilot contamination in IRS-assisted networks. It is noteworthy to mention that the pilot contamination problem also emerges from unwanted reflections during the channel estimation phase. The authors have proposed using orthogonal IRS configurations over time during the pilot transmission phase, which has been shown to remove or mitigate the negative effects of the operator coexistence in this phase. Another approach is proposed in [33], where the authors suggest fabricating ultra-narrowband metasurfaces to address the challenge. However, this solution is complex and contradicts the cost-efficiency of the IRS. Meanwhile, the authors in [34] study the system performance of a practical case with discrete phase shifts of the IRS in terms of inter-operator interference. The results show that the channel gain is reduced depending on the number of IRS

elements of the other operators in the presence of interoperator interference. In other words, the channel gain is no longer quadratic to the number of the IRS elements of the intended deployed IRS.

Other works in the literature tackle the frequency dependence of IRS reflections. A practical reflection model for a wideband IRS-assisted system is introduced in [35]. As an example, an element that generates 0° phase shift at  $2.4\,\mathrm{GHz}$  may introduce significantly different phase shifts at nearby frequencies, such as -100° at 2.5 GHz. Meanwhile, a novel channel estimation for a practical OFDM system is presented in [36], where it is taken in consideration that for wideband signals, the amplitude and phase shift of an element vary with different subcarriers. This phenomenon is also studied in multi-band scenarios. For instance, the authors in [37] propose a reflection model for signals at different frequencies and a joint transmit and IRS reflection beamforming design for power minimization and total SR maximization in a multi-cell multi-band system. Another joint optimization solution for BS-IRS-UE association, active beamforming at the BS and passive beamforming at IRS is provided in [38].

Following our previous studies on the coexistence issue of operators in IRS-assisted networks, one can argue that these challenges can be addressed by operator coordination and cooperation and effective spectrum-sharing protocols that consider cross-frequency impacts. In order to achieve this, some centralized control may be needed (see [39]), and operators may need to share information among each other

for a fair usage of the IRS as a resource. Other solutions utilizing machine learning tools may also be useful. For example, a deep reinforcement learning approach is proposed in [32], where an IRS provider dynamically allocates IRS resources to different operators. Additionally, regulatory frameworks may need to evolve to manage frequency coexistence, particularly as multi-operator, multi-IRSs environments become more common in 6G and beyond.

A summary of the proposed solutions toward unintended signal reflection in multi-operator IRS-assisted networks is given in Table 1. These solutions are mainly focused in the space and time domain, with their limitations being increased system complexity and necessity of operator coordination. It is obvious that spatial separation between deployed nodes also solves the problem; however, this not optimal and always feasible in reality. An alternative solution would be to "deactivate" the IRS when it is not in use by the intended operator, such as by employing an absorptive IRS as proposed in [31]. Although [31] primarily addresses spectral coexistence, its proposed concept can also be adapted to mitigate out-of-spectrum interference issues, by "switching on" the absorption mode of the IRS when it is not used by the intended operator. However, this approach would necessitate extensive coordination among operators, increasing system complexity and overhead.

#### 2.2. Previous Work for Narrowband Signals

Many studies on out-of-band impacts of IRS focus on single IRS setups or scenarios with two operators on different frequency bands. In contrast, our previous work addresses networks with five or more operators. The main concept involves dividing a single common IRS into multiple sub\_IRSs and dynamically assigning them to operators, while considering the impact on nearby operators as well. A schematic representation of this solution was shown in Fig. 1. The main idea is to understand whether the assignment has an impact in minimizing the negative effect of the unwanted reflections, denoted by the dashed arrows in the figure.

To assess the performance of this scheme, we rely on two key metrics: SR and Jain's Fairness Index (JFI). Our SNR formulation, detailed in [19, Section IV], calculates signal power by summing desired and undesired reflections, accounting for potential destructive interference. The system in [19] comprises of multiple operators (denoted as  $\mathcal{O}$ ) operating at adjacent mmWave frequencies, each with a single-antenna BS and UE and a centralized IRS. The IRS is divided equally among operators, such that each is served by an identical number of IRS elements. Experiments are conducted in Matlab, where we built a simple system level simulator. For each placement of communication nodes (a "single drop"), we calculate SR and JFI for a random subset of possible sub-IRS assignments ( $\mathcal{O}!$  (factorial) assignments are possible). For  $\mathcal{O} = 5$ , we compare the worst, average, and best assignments within this subset. Results show the best SR is six times higher than the worst case and twice

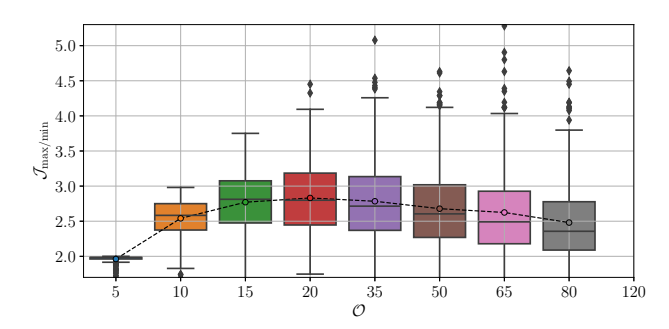


Figure 2: The impact of the number of operators on the gain from  $sub\_IRS$  assignment ([19, Section V]). The gain is indicated by  $\mathcal{J}_{max/min}$ , representing the JFI value of the best vs. the worst assignment of operators to the  $sub\_IRSs$ .

that of the average in 50% of cases. Moreover, the best JFI outcome also improves fairness among operators up to a value of about 0.9 (the fairest assignment would lead to a JFI value of 1).

Additional findings are concerned with the gain of sub\_IRS assignment. For the gain metric,  $\mathcal{J}_{\text{max/min}}$  is utilized, representing the improvement factor in terms of fairness between the best and worst sub\_IRS assignments. Here, JFI value is denoted by  $(\mathcal{J})$ . Results reveal that the gain from sub\_IRS assignment increases up to  $\mathcal{O} = 5$ , but diminishes as  $\mathcal{O}$  continues to grow (Fig. 2). This is expected, given that the number of elements in each sub\_IRS decreases as  $\mathcal{O}$  increases, leading to weaker unwanted reflections. Other results show that the gain also decreases at higher frequencies, likely due to narrower beam patterns. These findings are further expanded in [25], where we evaluate the benefits of sub\_IRS splitting in a system with multiple distributed IRSs, rather than a single centralized IRS. This configuration, where multiple IRSs are split into sub\_IRS units, outperforms both the centralized IRS setup and the conventional one-IRS-per-operator scenario. The enhanced flexibility in mitigating unwanted reflections through controlled sub-IRS assignment is a key reason for this improvement.

These previous works are developed under the assumption that network operators can share information with one another. Moreover, they include certain simplifying assumptions in the system model. First, we represent each operator by a BS and UE, each equipped with a single omnidirectional antenna. This assumption, however, does not hold for the mmWave band, where antenna arrays together with beamforming from transmitter (Tx) are typically required. Additionally, simulations only account for narrowband signals, for which the assumption for frequency-independent reflections actually holds. In this work, however, we loosen several assumptions that were previously imposed to simplify the system model. Specifically, this study includes beamforming at the transmitter side and considers wideband signals, which more closely reflect the characteristics of future networks.

To demonstrate that the coexistence problem can be

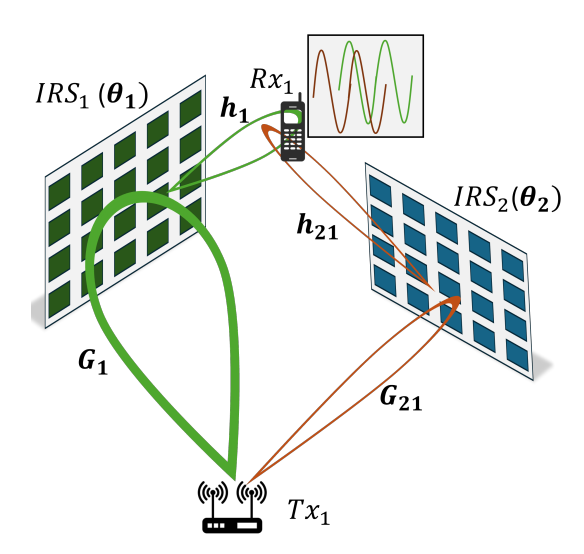


Figure 3: Illustration of the system model, where the two IRS are deployed by two different operators. The solid (wider) beams represent the desired path, whereas the dotted (narrower) ones represent the unwanted reflection.

naturally mitigated in wideband systems, we follow a two-step methodology. First, we analyze several characteristics of a multi-operator system using a simulation environment built in Matlab. Then, leveraging a 28 GHz testbed, we validate our findings by showing that the simulation results and real experimental data align well together.

# 3. System Model

# 3.1. Simulations

The system model is presented in Fig. 3, which demonstrates the coexistence of two operators, with the model easily extendable to more operators. For simplicity, we focus on the Tx and Rx of operator 1. This figure is a snapshot of the system model, and frequency indexing is omitted for readability purposes. Operator 1 has deployed IRS<sub>1</sub>, with its phase shift matrix denoted by  $\Theta_1[k]$ , where k is the subcarrier index. Tx<sub>1</sub> is beamforming the signal towards IRS<sub>1</sub>. The solid wider beams represent the desired signal path, with the channel matrices denoted by  $G_1[k]$ and  $h_1[k]$ . However, side lobes from  $Tx_1$  reach a nearby IRS, specifically IRS<sub>2</sub>, which is optimized for the frequency used by operator 2. The phase shift matrix for IRS<sub>2</sub> is denoted by  $\Theta_2[k]$ . The dotted narrower beams illustrate the unwanted reflection path, with the channel matrices for this path represented by  $G_{21}[k]$  and  $h_{21}[k]$ . As a result of these two paths, the signal reaching the receiver is represented as:

$$y_{1}[k] = (h_{1}[k]\Theta_{1}[k]G_{1}[k])s[k] + (h_{21}[k]\Theta_{2}[k]G_{21}[k])s[k] + n_{1}[k],$$
(1)

where s[k] is the transmitted signal at subcarrier k after precoding at the Tx. We assume the transmitted signal

satisfies  $\mathbb{E}\left[\|\mathbf{s}[k]\|^2\right] = P_{\text{sub}}$ , where  $P_{\text{sub}}$  is the transmit power allocated to subcarrier k. The total transmit power across all subcarriers, denoted by  $P_{\text{Tx}}$ , is related to  $P_{\text{sub}}$  by  $P_{\text{Tx}} = N_{\text{sub}} \cdot P_{\text{sub}}$ , where  $N_{\text{sub}}$  is the total number of active subcarriers. The term  $n_1[k] \sim \mathcal{CN}(0, \sigma_n^2)$  represents additive white Gaussian noise at subcarrier k. As illustrated at the top right of Fig. 3, depending on when these signals arrive at  $\text{Rx}_A$ , the dotted signal might have destructive impact on the solid signal. This equation can be further extended to a network consisting of more operators, as following:

$$y_{i}[k] = (\boldsymbol{h_{i}}[k]\boldsymbol{\Theta_{i}}[k]\boldsymbol{G_{i}}[k]) \boldsymbol{s}[k] + \sum_{\substack{j=1\\j\neq i}}^{\mathcal{O}} (\boldsymbol{h_{ij}}[k]\boldsymbol{\Theta_{j}}[k]\boldsymbol{G_{ij}}[k]) \boldsymbol{s}[k] + n_{i}[k], \quad (2)$$

where  $\mathcal{O}$  stands for the number of operators.

Given this model, we further evaluate how the this impact is related to the channel BW. The simulation environment is built upon the MATLAB example of IRS modeling, which is part of the 6G Exploration Library for 5G Toolbox [40].

The main characteristics of this model can be summarized as follows:

- The IRS channel is modeled as two concatenated clustered delay line (CDL) channels: Tx to IRS and IRS to Rx.
- The transmitted signal resembles a 6G-like signal, closely aligning with the 3rd generation partnership project (3GPP) specifications for 5G new radio (NR), with certain parameters extended beyond their defined ranges [41, 42].
- The phases of the elements of the IRS are controlled via an iterative algorithm, provided in [43]. This algorithm calculates the precoding vector and the phases of the IRS for maximizing the achievable rate, and it guarantees a locally optimal solution.
- The rest of the parameters defined in this example follow [21].

The parameters used for the multi-operator simulation are provided in Table 2, unless stated otherwise. Here,  $P_{Tx}$  stands for the transmitted power and  $\lambda$  for the signal's wavelength. Also, A stands for the amplitude of reflection of the IRS elements, and it is considered to be 0.8 (maximum value would be 1), in order to account for the practical hardware limitations and imperfections.  $d_x$  and  $d_y$  represent the width and length of each IRS element. It should be mentioned that the coefficients of the IRS are optimal for  $f_c$  instead of the frequencies occupied by the whole bandwidth [40, 43]. In other words, while the IRS phase shifts are ideal for the center frequency, their effectiveness decreases towards the edges of the band. It is

Parameter	Value
BW	$320\mathrm{MHz}$
Subcarrier spacing (SS)	$480\mathrm{kHz}$
Modulation	QPSK
Tx size	4 x 4
Rx size	1
IRS size	$10 \times 10$
$d_x$	$\lambda/5$
$d_y$	$\lambda/5$
A	0.8
$P_{Tx}$	$25\mathrm{dBm}$
Noise figure (NF)	$7\mathrm{dB}$
Thermal Noise Density	$\text{-}174\mathrm{dBm/Hz}$

Table 2: Table of parameters used in simulations.

noteworthy to mention that, while the default model of the two concatenated channels is CDL-A, we have used CDL-C to perform the simulations because CDL-A corresponds to a channel represented by a single tap, whereas CDL-C resembles a more realistic multipath channel model with multiple delay taps and varying power levels, better representing typical urban macrocell environments. Moreover, the example itself performs error-free perfect channel estimation; by directly computing the channel impulse response (CIR) and channel frequency response (CFR) based on the known channel model used in the simulation. However, in order to account for practical limitations, practical channel estimation is performed, which is done by using demodulation reference signal (DM-RS) as a received reference signal.

As an example, following the parameters mentioned above, the magnitude of the CFR of a IRS channel is shown in Fig. 4. The nodes are positioned randomly, with a maximum distance between Tx-IRS and IRS-Rx of 50 m. This plot shows the 40 MHz, 320 MHz, and 1.28 GHz channels, highlighting that the larger the BW, the more frequency selective the channel becomes. The image is zoomed in for the 40 MHz channel, in order to improve the readability of the plot. The perfect estimation result for 1.28 GHz is included for comparison. For the wider channel, variations of about 20 dB are observed, reducing to about 10 dB and 5 dB for the narrower channels, respectively. Notably, for a CDL-A-modeled IRS-assisted channel, the variation at 320 MHz is approximately 7–8 dB when all other parameters remain the same. It is clear that the wider the channel, the more does the BW exceed the coherence BW (the relative BW is increased as well), thus frequency selectivity becomes pronounced. Next, the plot in Fig. 5 shows the CFR from real measurements in a SDR-based built testbed, where the communication between the Tx and Rx is supported from a single NRRS (no LOS). The raw data is shown in a lighter color, while the darker red curve represents the result of applying a moving average filter to smooth the data. For a 320 MHz channel the observed

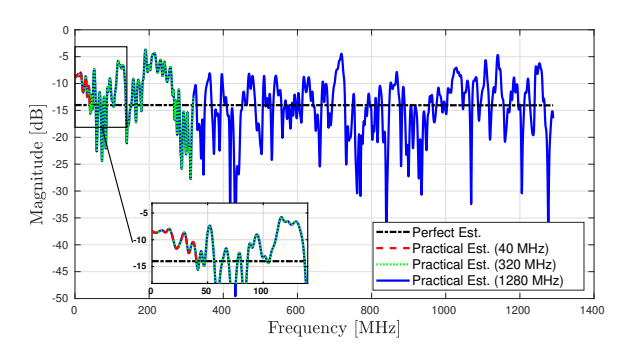


Figure 4: The magnitude of the CFR of a IRS-assisted channel for different BWs in simulations.

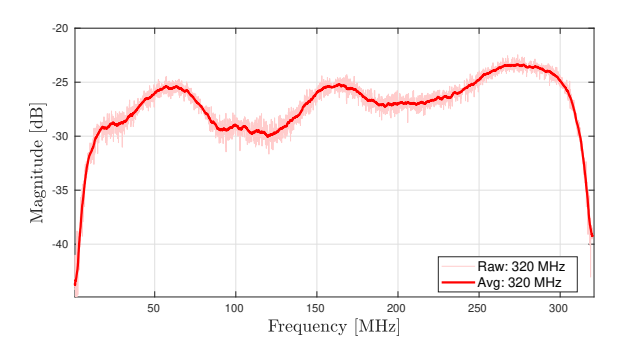


Figure 5: The magnitude of the CFR of a NRRS-assisted link from indoor measurements in the SDR-based built testbed.

frequency selectivity has a variation of about 10 dB.

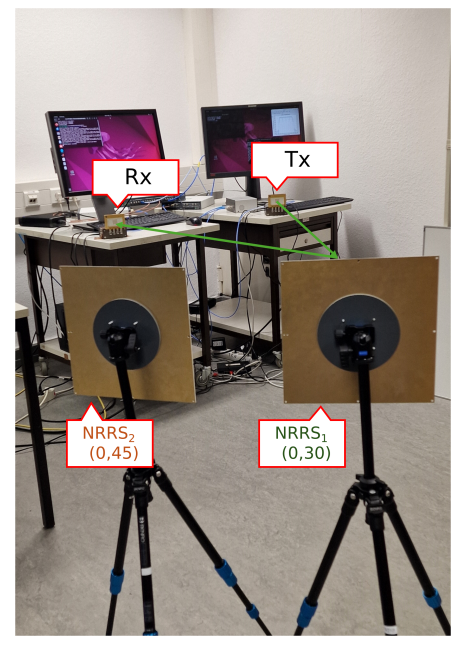


Figure 6: Experimental setup modeling the coexistence of two operators.

#### 3.2. Measurements

The testbed designed for this experiment operates in the 28 GHz spectrum. It comprises two SDRs and two NRRSs, as illustrated in Fig. 6. The SDRs, specifically USRPs X410 (National Instruments), have a master clock rate of 500 MHz and are configured at an intermediate frequency (IF) of 1 GHz. The stationary Tx and Rx are equipped with electronically steerable antenna arrays. These frontends are BBox Lite 5G units from TMYTEK, operating at 28 GHz and featuring a 3 dB beamwidth of 25°. Additionally, they are synchronized using the up/down converter (UD) Box from TMYTEK, which includes an OCXO reference clock. Two NRRSs, XRifle from TMYTEK, are used in this setup. These are passive devices pre-configured to reflect signals arriving at a specific angle towards another specific angle. Each NRRS operates has a frequency coverage between 26 GHz to 30 GHz, and provides a radar cross-section gain of approximately 70 dB. Finally, the SDRs are linked to two host computers equipped with AMD Ryzen 9 7950X processors via 100 Gbe Ethernet cables.

There are a few important setup details worth noting. First, the antennas are positioned to ensure there is no LOS communication path between them. In other words, signal reception occurs exclusively through the NRRS-assisted path. To model the first operator, NRRS<sub>1</sub> is selected and positioned such that its angles of arrival and departure are perfectly aligned with the frontends. The chosen angle configuration is INC: 0° and REF: 30°, where INC represents the incidence angle and REF the reflection angle. The second operator's impact on the signal of operator A is modeled by randomly placing a single NRRS nearby, selected from a set of seven different NRRSs. In essence, the influence of the second operator is considered as a random reflection affecting the first operator's communication. Thus, a randomly positioned NRRS is sufficient for modeling and analyzing the coexistence of two IRS-assisted operator networks. The chosen angle configuration for NRRS<sub>2</sub> is INC: 0° and REF: 45°. Moreover, the measurements are performed for random positions of this NRRS in the lab room, part of which is shown in Fig. 6. The random positions of the other NRRS emulates the impact of operators deployed spatially nearby.

For the software implementation, the MATLAB WLAN Toolbox is employed to generate an 802.11be OFDM waveform compliant with the extremely high throughput (EHT) standard defined in IEEE 802.11be. Without loss of generality, a WiFi waveform is used in the testbed implementation, even though the simulation is based on a 6G-like signal. This choice is made due to the structural similarity, as both are based on OFDM. The WLAN Toolbox in MATLAB provides an efficient way to generate and manipulate such waveforms, enabling flexible evaluation of system performance. The waveform is configured with a BW of 320 MHz and a modulation and coding scheme (MCS) index of 0, which specifies the use of binary phase shift keying (BPSK) modulation and a code rate of 1/2. The BW is the maximum possible BW supported by the SDR used in this

testbed. To ensure efficient transmission, the generated signal is normalized so that its peak amplitude is 1. The signal is then resampled from its baseband sampling rate using a 25/16 factor, aligning it with the hardware's sample rate requirements. The processed waveform is transmitted via the USRP in a continuous loop, ensuring reliable delivery across the channel.

On the receiver side, the USRP captures the transmitted signal at a sample rate of 500 MS/s, preserving the high-fidelity wideband characteristics. The captured signal undergoes post-processing in MATLAB, where it is resampled back using a 16/25 factor to match the original baseband rate. For each successfully detected packet, the channel characteristics are analyzed. The CFR is computed first, using the EHT-long training field (LTF) field, which is specifically designed for precise channel estimation in Wi-Fi 7 systems. The CIR is subsequently derived from the CFR, providing further insights into the multipath propagation effects experienced by the transmitted signal.

#### 4. Evaluation

# 4.1. Simulations

The simulation environment gives flexibility in terms of the reachable bandwidth, thus the simulations cover results from 10 MHz up to 1.28 GHz. The first set of results is obtained for the parameters provided in Table 2, by altering the BW and keeping power spectral density (PSD) fixed. The nodes of the two operators are randomly placed, ensuring a maximum distance of 50 m between the Tx-IRS and IRS-Rx of one operator. The path loss for the overall IRS-assisted channel is computed following the formula provided in [21]:

$$PL_{IRS} = \left(\frac{4\pi d_t d_r}{N_{IRS} d_x d_y A}\right)^2, \tag{3}$$

where  $d_t$  stands for the distance Tx-IRS,  $d_r$  stands for the distance IRS-Rx,  $N_{\rm IRS}$  stands for the total number of IRS elements. Following the formulation in Eq. (1), the SNR<sub>i</sub> value per subcarrier (the SNR at UE<sub>i</sub> considering coexistence for subcarrier k) is computed as following:

$$SNR_{i}[k] = \frac{P_{sub}}{\sigma_{n}^{2}} \left| \boldsymbol{h}_{i}[k] \boldsymbol{\Theta}_{i}[k] \boldsymbol{G}_{i}[k] + \sum_{\substack{j=1\\j \neq i}}^{N} \boldsymbol{h}_{ij}[k] \boldsymbol{\Theta}_{j}[k] \boldsymbol{G}_{ij}[k] \right|^{2}.$$
(4)

In case of two operators, we configure their respective carrier frequencies are configured as  $f_c^1 = 28 \, \mathrm{GHz}$  and  $f_c^2 = 28.2 \, \mathrm{GHz}$ . We have computed SNR<sub>1</sub> and the SNR<sub>1</sub> (without considering the unwanted reflections impact), which is given below:

$$SNR_{1}^{'}[k] = \frac{|\boldsymbol{h_{1}}[k]\boldsymbol{\theta_{1}}[k]\boldsymbol{G_{1}}[k]|^{2} \cdot P_{sub}}{\sigma_{n}^{2}}.$$
 (5)

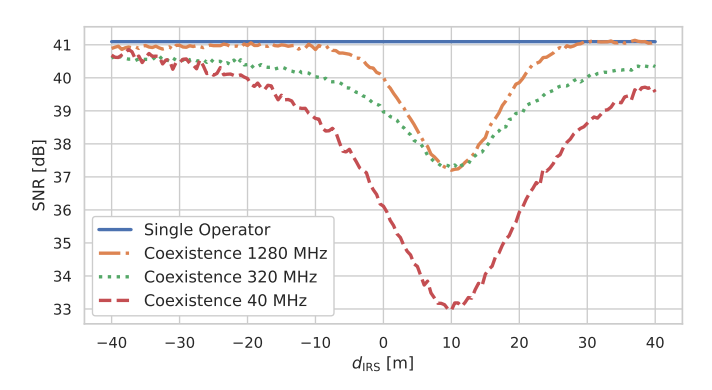


Figure 7: Impact of coexistence of two operators in SNR for different BWs. "No coexistence" curve corresponds to the case of a single operator.

To validate the simulation, a simple scenario is modeled in Matlab. Two operators, each deploying an IRS, are co-located initially. IRS<sub>1</sub> is then displaced along the x-axis, with d<sub>IRS</sub> representing the distance from IRS<sub>2</sub>. In Fig. 7, an example of how d<sub>IRS</sub> and BW impact the SNR<sub>1</sub> is shown. It is noteworthy to mention that this corresponds to a scenario where the unwanted reflection is causing destructive effect to SNR<sub>1</sub>, which is not always the case. The blue solid line illustrates SNR<sub>1</sub>, which is computed as the mean SNR across all subcarriers. In other words, this curve corresponds to the single operator case. Additionally, the mean SNR<sub>1</sub> is presented for three different BWs corresponding to this specific deployment scenario. This example can be used to draw two main conclusions. First of all, the coexistence issue is mitigated when the IRS nodes are placed sufficiently far apart, as expected. However, at certain distances, the SNR may be negatively impacted, as shown in the figure. Another interesting observation is that the variation in SNR impact diminishes with increasing BW. For a 40 MHz channel (dashed line), the maximum degradation is approximately 8 dB. In contrast, for a 1.28 GHz channel (dash-dotted line), this impact reduces to 3 dB and occurs over a smaller distance range compared to the 320 MHz case (dotted line).

Following these results and our hypothesis, we present findings for 500 different drops (i.e., node placements) of the coexistence scenario. Each drop represents a unique placement of the communication nodes, for which SNR<sub>1</sub> and SNR<sub>1</sub> are computed for various BWs. Building on the hypothesis that wider channels inherently reduce the impact of interference from other operators, it is anticipated that in this Monte Carlo simulation, the values of SNR<sub>1</sub> will show greater variability for narrower channels compared to wider ones. To investigate this, we first present the normalized variance of SNR<sub>1</sub> for channel bandwidths ranging from 10 MHz to 1.28 GHz. This is repeated for  $\mathcal{O}=2$  to  $\mathcal{O}=5$ , where  $\mathcal{O}$  is the number of operators. The plot in Fig. 8 confirms the hypothesis, as it reveals a clear decreasing trend from 10 MHz to 1.28 GHz channels. In essence, the plot shows that as BW increases, the

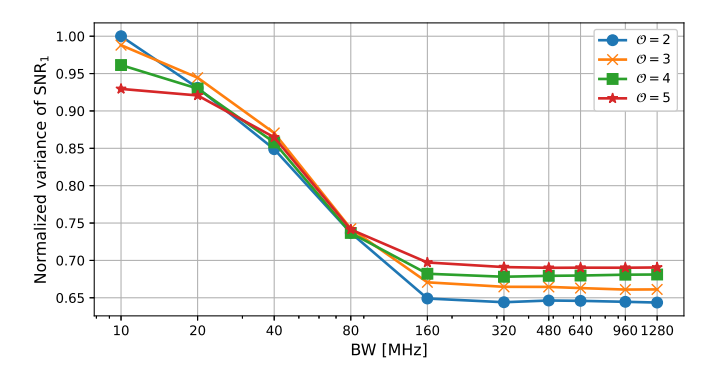


Figure 8: Normalized variance of  $SNR_1$  as a function of the BW.

SNR values show less deviation from the mean SNR, thus confirming the hypothesis about the averaging out effect of the SNR values among subcarriers. The variances are globally normalized, and as it can be seen, they increase as  $\mathcal{O}$  increases, and all values saturate after 160 MHz, since some expected variance comes from the randomness inherent in the Monte Carlo simulations. Additionally, all curves shift up as  $\mathcal{O}$  increases due to more unwanted reflections for each case. The x-axis in Fig. 8 is displayed on a logarithmic scale to improve readability across the wide range of channel BWs. We can conclude that in a scenario with two nearby operators, each deploying their own IRS, transmitting over channels slightly wider than 160 MHz is sufficient to ensure that they do not significantly impact each other's performance.

Next, to account for the variability in SNR<sub>1</sub> after excluding the outlier values, we calculate the 25th percentile (p25) and 75th percentile (p75) of the overall data. The difference between these percentiles gives the interquartile range (IQR) range. As shown in Fig. 9, the range of SNR<sub>1</sub> - depicted by the brightest shaded area, decreases as the BW increases, confirming that coexistence impacts become less significant at larger BWs. The IQR for the overall data - presented by the second darker shaded area, follows a similar trend. This is due to the channel affecting subcarriers differently, leading to a "balancing-out" effect that mitigates the overall impact on SNR across the wider BW. The range of SNR<sub>1</sub> is around 40 dB for a 10 MHz channel; dropping to around 20 dB for a BW of 1.28 GHz. The IQR range is also provided for the cases where the unwanted reflections have a destructive impact, namely, for the data where  $SNR_1 > SNR_1$ . Similarly, the darkest shaded area, presenting the IQR of the negatively impacted data, also narrows down for higher BWs. To summarize, the results confirm that the SNR in a network where multiple operators are coexisting and each deploys their own IRS is less variable for wideband channels.

### 4.2. Measurements

Since this paper focuses on comparing coexistence impacts as a function of channel BW, experiments for a

320 MHz channel are used and the narrower channels are emulated by selecting a subset of subcarriers from the 320 MHz channel. By emulating smaller BW values (e.g., 160 MHz, 80 MHz, down to 10 MHz) from the 320 MHz measurements, this approach ensures consistency across experiments while minimizing hardware reconfigurations. This method allows for a controlled comparison of coexistence impacts across different bandwidths, as the derived measurements inherently maintain the same environmental and multipath conditions observed during the original 320 MHz capture. The emulation process is achieved by isolating subsequent subcarrier subsets of the spectrum in the frequency domain to represent the desired BW, such as retaining only half of the subcarriers for 160 MHz out of the number of subcarriers used for 320 MHz.

First and foremost, we perform 29 different measurements: one of them when only the perfectly aligned NRRS is positioned, and the 28 other ones are corresponding to a perfectly placed NRRS and another randomly positioned NRRS in the room. In all the cases, the SNR of the received signal at the Rx USRP is computed. It should be noted that each trace is 0.1 s long and the SNR is computed across all received packets ( $\sim 700$  packets per trace), and the final value is the median of all the values. This process is repeated by considering the full number of subcarriers for 320 MHz (4096) and then halving it until 128 subcarriers (10 MHz).

We compute SNR<sub>1</sub> and the plot summarizing the results is presented in Fig. 10. The second darker shaded region represents the IQR range of the SNR<sub>1</sub> values across the 29 collected measurements. The lighter area encompasses the whole range across all data. Consistent with the simulation results, the variation in SNR decreases as the BW increases. For instance, the variation for a 10 MHz channel is approximately 10 dB, whereas for a 320 MHz channel, the variation reduces to about 3 dB. Since in some of the cases the impact of coexistence is positive towards SNR<sub>1</sub>, we again show the IQR of the negatively impacted data. The IQR exhibits a similar behavior, as it is shown by the darkest shaded area in the plot. The curve shows slight fluctuations due to the limited number of measurements from the testbed; however, the data is sufficient to

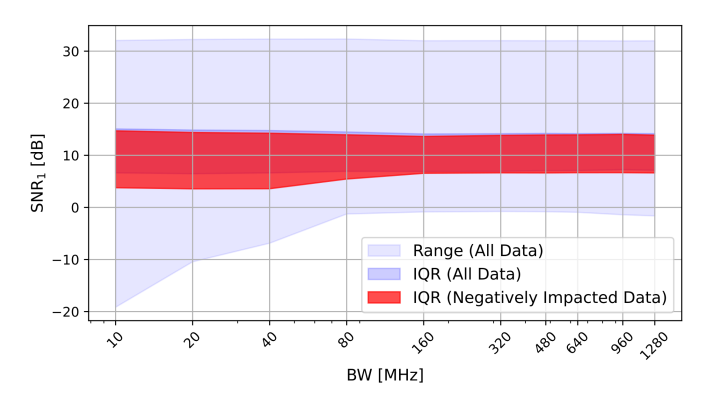


Figure 9: SNR distribution in simulations.

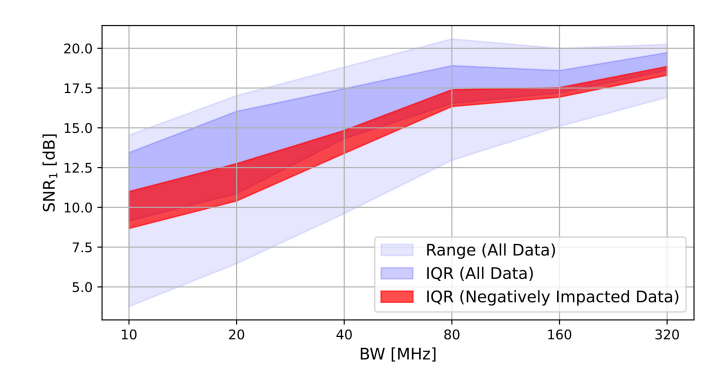


Figure 10: SNR distribution in real measurements.

observe the overall trend. The difference in the  $\rm SNR_1$  level is due to the emulation of smaller BWs from the 320 MHz measurements.

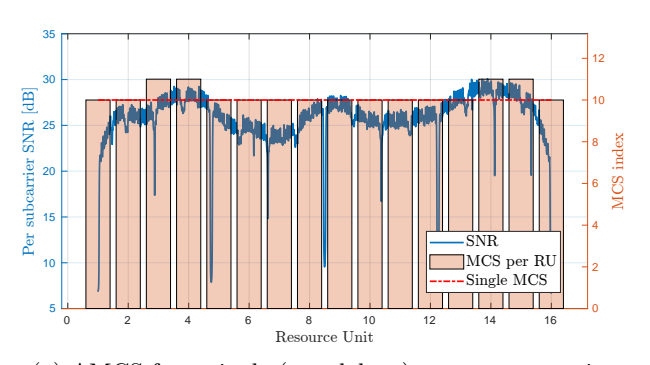
The results presented above demonstrate that frequencyselective wideband IRS-assisted channels effectively mitigate operator coexistence issues. However, difficulties arise for such frequency-selective channels, given that the SNR variation is of more than 15 dB. Thus, sophisticated PHY layers are necessary to ensure successful data transmission. Although this increased complexity may lead to higher power consumption at the receiver, it is important to note that such processing is typically performed by existing hardware components that are already active in conventional systems. Therefore, while there may be a modest increase in computational load, the overall energy efficiency gain achieved through the IRS remains substantial. As a subsequent step, we analyze how adaptive modulation and coding schemes (AMCSs) enhance channel performance under coexistence conditions and investigate how the AMCS gain is influenced by varying BWs. Using the provided measurement traces and the physical layer abstraction outlined in [44], we compute the data rate for each trace under two scenarios: first, where the optimal MCS is selected uniformly across all resource units (RUs) of the 320 MHz channel; and second, where the optimal MCS is selected independently for each RU. One RU contains 256 subcarriers, thus each RU is of 20 MHz BW. This analysis allows us to quantify the AMCS gain. We first present results that show how the coexistence of two NRRSs increases the frequency selectivity of the channel. Comparing Fig. 11a and Fig. 11b, it is clearly visible that coexistence of multiple NRRSs increases the frequency selectivity of the channel. Thus, the AMCS gain increases as well; namely from 1.67% in Fig. 11a, to 7.2% in Fig. 11b. In this case, the coexistence of the NRRSs has also decreased the overall quality of the received signal. The overall rate after AMCS for the standalone scenario is about 40.5% higher than that of the coexistence case after AMCS.

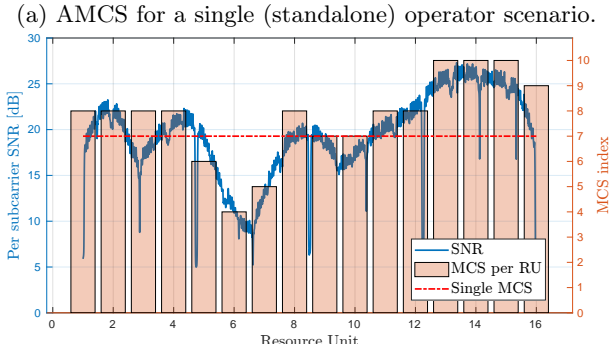
Next, we segment each trace into smaller BWs, following the same procedure as before, and compute the AMCS gain for channels ranging from  $20\,\mathrm{MHz}$  (16 RUs) up to  $160\,\mathrm{MHz}$  (2 RUs). The corresponding results are presented in Fig. 12.

As anticipated, the AMCS gain decreases for smaller BWs because the channel exhibits reduced frequency selectivity. In certain instances, a negative gain is observed, which occurs when the metric values are close but do not surpass the threshold required to select a higher MCS, resulting in a lower MCS being assigned per RU.

#### 5. Conclusion and Discussions

Building on our previous work on mitigating interoperator interference in IRS-assisted networks, this paper explores a wideband channel approach. Our key observation is that in wideband transmissions, the effect of unwanted reflections becomes less significant, as some subcarriers remain unaffected and can compensate for those that experience degradation. We validate this behavior both through simulations and real-world testbed measurements in the 28 GHz band. In both cases, we observe a consistent trend: the overall SNR exhibits reduced variance as BW increases. It is noteworthy to mention that our experimental setup employs NRRS, which operates similarly to IRS, but it is pre-configured and cannot be reconfigured over time. However, the solution can be generalized to fully reconfigurable IRS as well. This is because the frequency selectivity of a wideband channel, which is central to our analysis, is independent of the reconfigurability of the surface. The underlying reflection principles remain unchanged, and thus the observed trends are applicable to IRS design as well. Qualitative results are presented as well, which can be useful in network design. For example,





(b) AMCS for a coexistence scenario (two NRRSs).

Figure 11: Comparison of AMCS between the standalone and the coexistence scenario.

when two spatially close operators deploy each their own IRS, their interference to each other can be neglected if they transmit using channels slightly wider than 160 MHz.

Following the results presented in our study, the impact of operator coexistence and out-of-intended-band reflections in future multi-IRS-assisted networks cannot be neglected. As the landscape of wireless communication evolves, the design and operation of such networks will depend heavily on various factors, including deployment scenarios (indoor vs. outdoor), spectrum (mmWave vs. sub-6 GHz), BW characteristics and the capabilities of IRS itself. In some scenarios, such as environments requiring high-throughput and low-latency communication, adopting a wideband approach may prove to be the most feasible solution. This would enable the network to handle diverse applications and maintain performance even under coexistence constraints. However, in other cases, particularly where spatial freedom can be exploited, advanced beamforming and intelligent placement of IRS nodes could provide a more efficient alternative by minimizing interference and optimizing efficiency. Additionally, operator cooperation may also be required as IRS technology continues to evolve.

Collaborative approaches, such as the establishment of shared control mechanisms or dynamic spectrum-sharing agreements, may help mitigate coexistence challenges. The introduction of a centralized broker or mediator system to manage resource allocation and IRS assignments could further enhance the efficiency of coexistence strategies. Such a broker could dynamically adapt resource assignments based on real-time network demands, ensuring equitable access to resources while minimizing conflicts between operators. Continued advancements in IRS prototypes, combined with innovative policy and technological solutions, will play a crucial role in determining the most effective strategies for managing coexistence in multi-operator environments.

Alongside the aforementioned directions, this work particularly opens several directions for future research. One is to investigate dynamic IRS reconfiguration in wideband multi-operator scenarios, considering how real-time control, latency, and signaling overhead influence the mitigation of unwanted reflections. Another promising direction is

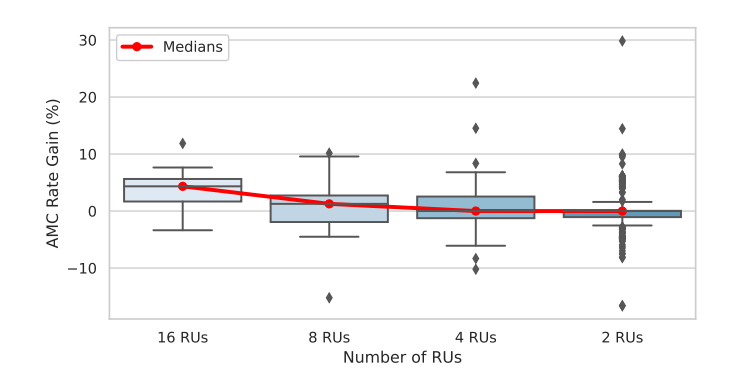


Figure 12: AMCS gain for different number of RUs.

the joint optimization of IRS configuration and opportunistic scheduling in multi-user settings, which could further enhance overall network performance.

#### Acknowledgments

This work was supported by the Federal Ministry of Education and Research (BMBF, Germany) within the 6G Research and Innovation Cluster 6G-RIC under Grant 16KISK020K.

# References

- Anutusha Dogra, Rakesh Kumar Jha, and Shubha Jain. A Survey on Beyond 5G Network With the Advent of 6G: Architecture and Emerging Technologies. *IEEE Access*, pages 67512 – 67547, October 2020. ISSN 2169-3536. doi: 10.1109/ACCESS.2020. 3031234
- [2] Wijdan K. Alsaedi, Hamed Ahmadi, Zaheer Khan, and David Grace. Spectrum Options and Allocations for 6G: A Regulatory and Standardization Review. *IEEE Open Journal of the* Communications Society, pages 1787–1812, August 2023. ISSN 2644-125X. doi: 10.1109/OJCOMS.2023.3301630.
- [3] Wei Hong, Zhi Hao Jiang, Chao Yu, Debin Hou, Haiming Wang, Chong Guo, Yun Hu, Le Kuai, Yingrui Yu, Zhengbo Jiang, Zhe Chen, Jixin Chen, Zhiqiang Yu, Jianfeng Zhai, Nianzu Zhang, Ling Tian, Fan Wu, Guangqi Yang, Zhang-Cheng Hao, and Jian Yi Zhou. The Role of Millimeter-Wave Technologies in 5G/6G Wireless Communications. IEEE Journal of Microwaves, pages 101–122, January 2021. ISSN 2692-8388. doi: 10.1109/ JMW.2020.3035541.
- [4] Satoshi Suyama, Tatsuki Okuyama, Nobuhide Nonaka, and Takahiro Asai. Recent Studies on Massive MIMO Technologies for 5G Evolution and 6G. In *IEEE Radio and Wireless Sympo*sium (RWS 2022), pages 90–93, Las Vegas, NV, February 2022. doi: 10.1109/RWS53089.2022.9719949.
- [5] Sohail Payami, Mohsen Khalily, Ali Araghi, Tian Hong Loh, David Cheadle, Konstantinos Nikitopoulos, and Rahim Tafazolli. Developing the First mmWave Fully-Connected Hybrid Beamformer With a Large Antenna Array. *IEEE Ac*cess, pages 141282–141291, July 2020. ISSN 2169-3536. doi: 10.1109/ACCESS.2020.3013539.
- [6] Binqi Yang, Zhiqiang Yu, Ji Lan, Ruoqiao Zhang, Jianyi Zhou, and Wei Hong. Digital Beamforming-Based Massive MIMO Transceiver for 5G Millimeter-Wave Communications. *IEEE Transactions on Microwave Theory and Techniques*, pages 3403–3418, July 2018. ISSN 0018-9480. doi: 10.1109/TMTT.2018. 2829702.
- [7] Sherif Adeshina Busari, Kazi Mohammed Saidul Huq, Shahid Mumtaz, Linglong Dai, and Jonathan Rodriguez. Millimeter-Wave Massive MIMO Communication for Future Wireless Systems: A Survey. *IEEE Communications Surveys & Tutorials*, pages 836–869, December 2017. ISSN 1553-877X. doi: 10.1109/COMST.2017.2787460.
- [8] Cunhua Pan, Hong Ren, Kezhi Wang, Jonas Florentin Kolb, Maged Elkashlan, Ming Chen, Marco Di Renzo, Yang Hao, Jiangzhou Wang, A. Lee Swindlehurst, Xiaohu You, and Lajos Hanzo. Reconfigurable Intelligent Surfaces for 6G Systems: Principles, Applications, and Research Directions. *IEEE Com*munications Magazine, 59(6):14–20, June 2021. ISSN 0163-6804. doi: 10.1109/MCOM.001.2001076.
- [9] Ertugrul Basar, Marco Di Renzo, Julien de Rosny, Merouane Debbah, Mohamed-Slim Alouini, and Rui Zhang. Wireless Communications Through Reconfigurable Intelligent Surfaces. *IEEE Access*, pages 116753–116773, August 2019. ISSN 2169-3536. doi: 10.1109/ACCESS.2019.2935192.

- [10] Xilong Pei, Haifan Yin, Li Tan, Lin Cao, Zhanpeng Li, Kai Wang, Kun Zhang, and Emil Björnson. RIS-Aided Wireless Communications: Prototyping, Adaptive Beamforming, and Indoor/Outdoor Field Trials. *IEEE Transactions on Communications*, 69(12):8627–8640, 2021. ISSN 1558-0857. doi: 10.1109/TCOMM.2021.3116151.
- [11] ETSI. Reconfigurable Intelligent Surfaces (RIS); Implementation and Practical Considerations. GR RIS 004 V1.1.1, European Telecommunications Standards Institute, March 2025. URL https://www.etsi.org/deliver/etsi\_gr/RIS/001\_099/004/01.01.01\_60/gr\_RIS004v010101p.pdf#page=54.09.
- [12] Kun Qian, Lulu Yao, Xinyu Zhang, and Tse Nga Ng. MilliMirror: 3D printed reflecting surface for millimeter-wave coverage expansion. In 28th ACM International Conference on Mobile Computing and Networking (MobiCom 2022), pages 15–28, Sydney, Australia, October 2022. ACM. ISBN 978-1-4503-9518-2. doi: 10.1145/3495243.3517024.
- [13] Markus Heinrichs, Aydin Sezgin, and Rainer Kronberger. Open Source Reconfigurable Intelligent Surface for the Frequency Range of 5 GHz WiFi. In *IEEE International Symposium On Antennas And Propagation (ISAP 2023)*, Kuala Lumpur, Malaysia, January 2023. doi: 10.1109/ISAP57493.2023.10389095.
- [14] Robin Neuder, Marc Späth, Martin Schüßler, and Alejandro Jiménez-Sáez. Architecture for sub-100 ms liquid crystal reconfigurable intelligent surface based on defected delay lines. Communications Engineering, May 2024. ISSN 2731-3395. doi: 10.1038/s44172-024-00214-3.
- [15] Emil Björnson, Özgecan Özdogan, and Erik G. Larsson. Reconfigurable Intelligent Surfaces: Three Myths and Two Critical Questions. *IEEE Communications Magazine*, pages 90–96, December 2020. ISSN 0163-6804. doi: 10.1109/MCOM.001.2000407.
- [16] Huiying Jiao, Hui Liu, and Zhiqin Wang. Reconfigurable Intelligent Surfaces aided Wireless Communication: Key Technologies and Challenges. In 18th IEEE International Conference on Wireless and Mobile Computing (IWCMC 2022), Dubrovnik, Croatia, May 2022. doi: 10.1109/IWCMC55113.2022.9824117.
- [17] Hamed Radpour, Markus Hofer, Lukas Walter Mayer, Andreas Hofmann, Martin Schiefer, and Thomas Zemen. Active Reconfigurable Intelligent Surface for the Millimeter-Wave Frequency Band: Design and Measurement Results. In *IEEE Wireless Com*munications and Networking Conference (WCNC 2024), Dubai, United Arab Emirates, April 2024. doi: 10.1109/WCNC57260. 2024.10571022.
- [18] A. Lee Swindlehurst, Gui Zhou, Rang Liu, Cunhua Pan, and Ming Li. Channel Estimation With Reconfigurable Intelligent Surfaces—A General Framework. Proceedings of the IEEE, pages 1312–1338, September 2022. ISSN 0018-9219. doi: 10. 1109/JPROC.2022.3170358.
- [19] Joana Angjo, Anatolij Zubow, and Falko Dressler. Side Effects of IRS: On the Need for Coordination in 6G Multi-Operator IRS-assisted Networks. In *IEEE Global Communications Conference (GLOBECOM 2023)*, 4th Workshop on Emerging Topics in 6G Communications (6GComm 2023), pages 1380–1385, Kuala Lumpur, Malaysia, December 2023. IEEE. doi: 10.1109/GCWkshps58843.2023.10464696.
- [20] Yusuf Olayinka Imam-Fulani, Nasir Faruk, Olugbenga A. Sowande, Abubakar Abdulkarim, Emmanuel Alozie, Aliyu D. Usman, Kayode S. Adewole, Abdulkarim A. Oloyede, Haruna Chiroma, Salisu Garba, Agbotiname Lucky Imoize, Bashir Abdullahi Baba, Abdulwaheed Musa, Yinusa A. Adediran, and Lawan S. Taura. 5G Frequency Standardization, Technologies, Channel Models, and Network Deployment: Advances, Challenges, and Future Directions. Sustainability, March 2023. ISSN 2071-1050. doi: 10.3390/su15065173.
- [21] ETSI. Reconfigurable Intelligent Surfaces (RIS); Communication Models, Channel Models, Channel Estimation and Evaluation Methodology. GR RIS 003 V1.1.1, European Telecommunications Standards Institute, June 2023. URL https://www.etsi.org/deliver/etsi\_gr/RIS/001\_099/003/01.01.01\_60/gr\_RIS003v010101p.pdf.
- [22] Samara Gharbieh, Raffaele D'Errico, and Antonio Clemente.

- Reconfigurable Intelligent Surface Design using PIN Diodes via Rotation Technique Proof of Concept. In 17th European Conference on Antennas and Propagation (EuCAP 2023), Florence, Italy, March 2023. IEEE. doi: 10.23919/eucap57121.2023. 10133091.
- [23] Pantelis Koutroumpis, Pau Castells, and Kalvin Bahia. To share or not to share? The impact of mobile network sharing for consumers and operators. *Information Economics and Policy*, 65, December 2023. ISSN 0167-6245. doi: 10.1016/j.infoecopol. 2023.101061.
- [24] Garrett Hardin. The Tragedy of the Commons. Science, 162 (3859):1243–1248, December 1968. ISSN 1095-9203. doi: 10. 1126/science.162.3859.1243.
- [25] Joana Angjo, Nikolaos Athanasiadis, Anatolij Zubow, and Falko Dressler. Improving Multi-Operator Coexistence in Distributed-IRS Assisted Networks. In *European Wireless (EW 2024)*, pages 7–12, Brno, Czechia, September 2024.
- [26] Beixiong Zheng, Changsheng You, and Rui Zhang. Fast Channel Estimation for IRS-Assisted OFDM. IEEE Wireless Communications Letters, 10(3), March 2021. ISSN 2162-2337. doi: 10.1109/LWC.2020.3038434.
- [27] Ruiqi Wang, Yiming Yang, Behrooz Makki, and Atif Shamim. A Wideband Reconfigurable Intelligent Surface for 5G Millimeter-Wave Applications. *IEEE Transactions on Antennas and Prop*agation, 72(3):2399–2410, March 2024. ISSN 0018-926X. doi: 10.1109/TAP.2024.3352828.
- [28] Yajun Zhao and Xin Lv. Network Coexistence Analysis of RIS-Assisted Wireless Communications. *IEEE Access*, 10:63442–63454, 2022. ISSN 2169-3536. doi: 10.1109/access.2022.3183139.
- [29] Doğa Gürgünoğlu, Emil Björnson, and Gábor Fodor. Impact of Pilot Contamination Between Operators With Interfering Reconfigurable Intelligent Surfaces. In *IEEE International Black Sea Conference on Communications and Networking* (BlackSeaCom 2023), Istanbul, Turkey, July 2023. IEEE. doi: 10.1109/blackseacom58138.2023.10299699.
- [30] Doğa Gürgünoğlu, Emil Björnson, and Gábor Fodor. Combating Inter-Operator Pilot Contamination in Reconfigurable Intelligent Surfaces Assisted Multi-Operator Networks. *IEEE Transactions* on Communications, 72(7):5884–5895, July 2024. ISSN 1558-0857. doi: 10.1109/TCOMM.2024.3390095.
- [31] Fangzhou Wang and A. Lee Swindlehurst. Applications of Absorptive Reconfigurable Intelligent Surfaces in Interference Mitigation and Physical Layer Security. *IEEE Transactions on Wireless Communications*, 23(5):3918–3931, May 2024. ISSN 1536-1276. doi: 10.1109/TWC.2023.3312693.
- [32] Haocheng Zhang, Wei Wang, Hao Zhou, Zhiping Lu, and Ming Li. A Hierarchical DRL Approach for Resource Optimization in Multi-RIS Multi-Operator Networks. eess.sy, arXiv, October 2024.
- [33] Mehdi Monemi, Mehdi Rasti, Arthur S. de Sena, Mohammad Amir Fallah, Matti Latva-aho, and Marco Di Renzo. Practical Challenges for Reliable RIS Deployment in Heterogeneous Multi-Operator Multi-Band Networks. eess.sy, arXiv, January 2025.
- [34] Nikolaos I. Miridakis, Theodoros A. Tsiftsis, Panagiotis A. Karkazis, Helen C. Leligou, and Petar Popovski. Impact of Inter-Operator Interference via Reconfigurable Intelligent Surfaces. IEEE Wireless Communications Letters, 13(9):2536–2540, September 2024. ISSN 2162-2337. doi: 10.1109/LWC.2024.3425728.
- [35] Wenhao Cai, Hongyu Li, Ming Li, and Qian Liu. Practical Modeling and Beamforming for Intelligent Reflecting Surface Aided Wideband Systems. *IEEE Communications Letters*, 24(7): 1568–1571, July 2020. ISSN 1558-2558. doi: 10.1109/LCOMM. 2020.2987322.
- [36] Wanning Yang, Hongyu Li, Ming Li, Yang Liu, and Qian Liu. Channel Estimation for Practical IRS-Assisted OFDM Systems. In IEEE Wireless Communications and Networking Conference (WCNC 2021), WCNC Workshops 2021 (Workshops), Nanjing, China, March 2021. doi: 10.1109/WCNCW49093.2021.9419982.
- [37] Wenhao Cai, Rang Liu, Ming Li, Yang Liu, Qingqing Wu, and

- Qian Liu. IRS-Assisted Multicell Multiband Systems: Practical Reflection Model and Joint Beamforming Design. *IEEE Transactions on Communications*, 70(6):3897–3911, June 2022. ISSN 1558-0857. doi: 10.1109/TCOMM.2022.3168645.
- [38] Sifan Liu, Rang Liu, Ming Li, Yang Liu, and Qian Liu. Joint BS-RIS-User Association and Beamforming Design for RIS-assisted Cellular Networks. *IEEE Transactions on Vehicular Technology*, 72(5):6113–6128, May 2023. ISSN 1939-9359. doi: 10.1109/TVT. 2022.3231347.
- [39] Stefan Schwarz. Gambling on Reconfigurable Intelligent Surfaces. IEEE Communications Letters, 28(4), January 2024. ISSN 1558-2558. doi: 10.1109/LCOMM.2024.3360477.
- [40] Model Reconfigurable Intelligent Surfaces with CDL Channels. https://de.mathworks.com/help/5g/ug/model-reconfigurable-intelligent-surfaces-with-cdl-channels.html, 2025.
- [41] NR; Radio Resource Control (RRC) protocol specification. TS 38.331 v16.1.0, 3rd Generation Partnership Project, June 2025.
- [42] NR; Physical channels and modulation. TS 38.211 v19.0.0, 3rd Generation Partnership Project, June 2025.
- [43] Tao Zhou and Kui Xu. Multi-Intelligent Reflecting Surface-Aided Wireless Network With Achievable Rate Maximization. In International Conference on Wireless Communications and Signal Processing (WCSP 2020), Nanjing, China, October 2020. doi: 10.1109/WCSP49889.2020.9299714.
- [44] 802.11ax PHY-Focused System-Level Simulation https://de.mathworks.com/help/wlan/ug/802-11ax-phy-focused-system-level-simulation.html, 2025.